

Fig. 8. EBSD investigation of a partially transformed bainite packet. MI cycle interrupted after 45% transformation. (a) Light micrograph (nital etching). (b) $\{001\}_\alpha$ pole figure showing that non-parallel sets labelled 1, 2 and 3 all belong to the same Bain zone of the former austenite grain.

were investigated using EBSD. As illustrated in Fig. 8, the non-parallel sets of groups always belong to the same Bain zone of the former austenite grain. As a consequence, after thickening of the sets of groups into packets, many low angle boundaries are found in the misorientation angle histograms (Fig. 6(a)). These are not easily visible after metallographic etching, so that the fully transformed microstructures appear to be “granular” and irregularly shaped. Due to the incomplete transformation phenomenon and to the intricate morphology of the groups, equiaxed, carbon-rich M–A particles are found between groups, within the packets. This complex structure and shape of bainite packets had already been observed in a detailed three-dimensional study [35]. These features could also be recognised in previous studies of “granular” or even “rectangular” [36] bainite microstructures, e.g., Fig. 8 in [37], Figs. 4, 8, 14(a) and (b) in [38], Fig. 11(b) in [39], Fig. 3 in [28] (obtained with in situ observations), and also possibly Fig. 16(a) in [40] and Fig. 1(b) in [24].

The formation of straight groups, followed by slower thickening of groups into packets could possibly be explained by considering the mechanism proposed by Ohmori et al. [28], i.e., a “martensitic-like” transformation followed by diffusion-assisted thickening. Nevertheless, this model does not consider the spatial and crystallographic configuration of bainite groups, which, in the microstructures investigated here, greatly differs from the parallel-shaped, twin-related “covariant packets” found in martensite [7,12]. In addition, other factors, including the strength of the mother austenite phase, could also influence the morphology of the bainite groups.

4.1.2. Consequences on the resistance to brittle cleavage fracture

In the fully transformed microstructures, high-angle boundaries observed in the EBSD maps (white lines in Fig. 4) delimit the “crystallographic packets” [7,8], which are the “effective packets” regarding cleavage crack propagation [8,11]. These packets are very intricate and non-convex, in particular in the MI microstructure. Due to the transformation mechanism evidenced here, and as shown in Fig. 9, crystallographic packets (‘a + b’ and ‘c’) do not necessarily correspond to morphological packets (‘a’ and ‘b + c’). Actually, crystallographic packets frequently consist of several morphological packets. This could explain why in upper bainite cleavage microcracks often propagate without significant deviation over several morphological packets [5]. As a result, both HI and MI microstructures are more sensitive to brittle cleavage fracture than the base metal, with impact toughness transition temperatures (at 70 J) of -89 , -31 and $+15$ °C for the base metal, MI (intricate) and HI (coarser) microstructures, respectively [9]. This is due, at least in part, to the coarse bainite matrix [41]. The mechanism of variant selection, leading to numerous low angle boundaries and thus to coarse crystallographic packets, is still unclear. In this study,

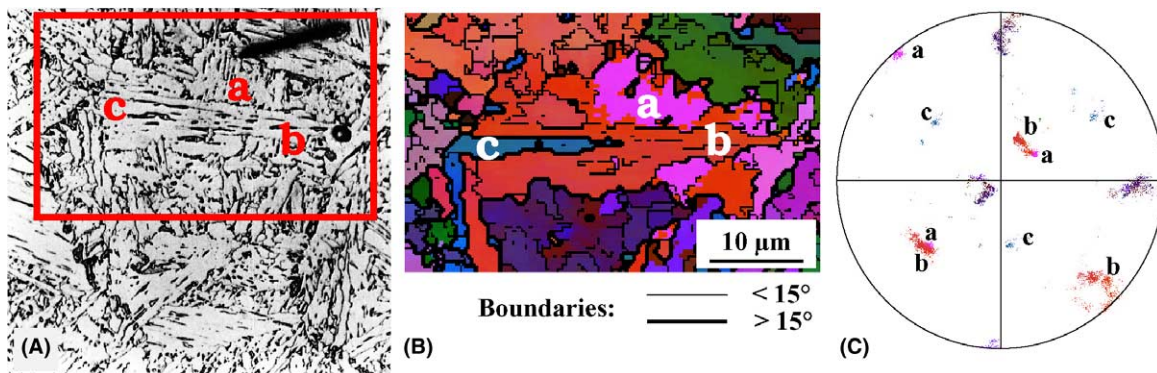


Fig. 9. High-magnification light micrograph (A) and corresponding EBSD map (B) showing that morphological packets (“a” and “b + c”) do not match crystallographic packets delimited by high-angle boundaries (“a + b” and “c”). (C) Corresponding $\{001\}_\alpha$ pole figure showing high misorientation between crystallographic packets.